Bioorganic & Medicinal Chemistry 18 (2010) 1356–1363

Contents lists available at ScienceDirect

Bioorganic & Medicinal Chemistry

journal homepage: www.elsevier.com/locate/bmc

Site-specific labeling of 'second generation' annexin V with $^{99m}Tc(CO)_3$ for improved imaging of apoptosis in vivo

Marijke De Saint-Hubert [a], Felix M. Mottaghy [a], Kathleen Vunckx [a], Johan Nuyts [a], Humphrey Fonge [b], Kristof Prinsen [b], Sigrid Stroobants [a], Luc Mortelmans [a], Niko Deckers [c], Leo Hofstra [c], Chris P. M. Reutelingsperger [c], Alfons Verbruggen [b,*], Dirk Rattat [b]

[a] Department of Nuclear Medicine, University Hospital Gasthuisberg Leuven, Herestraat 49, B-3000 Leuven, Belgium
[b] Laboratory for Radiopharmacy, Faculty of Pharmaceutical Sciences, K.U. Leuven, O&N 2, Box 821, Herestraat 49, B-3000 Leuven, Belgium
[c] Department of Biochemistry, University Maastricht, NL-6200 Maastricht, Netherlands

ARTICLE INFO

Article history:
Received 17 July 2009
Revised 6 December 2009
Accepted 8 December 2009
Available online 5 January 2010

Keywords:
Annexin V
Apoptosis
Technetium-99m
Tricarbonyl labeling
Imaging

ABSTRACT

In this study 'second generation' AnxV was specifically labeled with ^{99m}Tc in three different ways outside the binding region of the protein to obtain an improved target-to-background activity ratio. The compounds were tested in vitro and in vivo in normal mice and in a model of hepatic apoptosis (anti-Fas mAb). The apoptosis binding was most prominent for the HIS-tagged 'second generation' AnxV labeled with $^{99m}Tc(CO)_3$ in comparison to ^{99m}Tc-HYNIC-*cys*-AnxV and $^{99m}Tc(CO)_3$-DTPA-*cys*-AnxV.

1. Introduction

Apoptosis, or programmed cell death, plays an essential role in the development and maintenance of a multicellular organism and contributes to normal physiology and pathology.[1]

Abundant apoptosis occurs in several pathologies[2] as in the case of organ rejection[3] and cardiovascular[4] and neurodegenerative diseases.[5] Insufficient apoptosis can be seen in malignant processes.[6] Therefore, some new anti-cancer therapies focus on induction of apoptosis. Resistance to apoptosis can be a cause of therapy failure.[7] Imaging of therapy induced apoptosis offers a new way to assess tumor response directly and in an early stage of therapy,[8] in this way allowing an optimal individualized treatment strategy.

One of the hallmarks of cells going into apoptosis is the externalization of the phospholipid phosphatidylserine (PS) at the cell membrane.[9] Annexin A5 (AnxV A5), a 36-kDa human protein, shows Ca^{2+}-dependent binding to negatively charged phospholipid surfaces and was discovered as vascular anticoagulant protein (VAC-α or AnxV). The anticoagulant activity is based on the high-affinity for PS.[10,11] These characteristics make a derivative of AnxV a suitable candidate for imaging of apoptosis.

Several fluorescent or radiolabeled AnxV derivatives have already been studied.[12–15] Technetium-99m radiolabeled hydrazinonicotinamide-AnxV (HYNIC-AnxV) has been proposed for molecular imaging of apoptosis and first clinical data of ^{99m}Tc-HYNIC-AnxV have already been published.[16–18] However, the target-to-background activity ratio is rather low.[19–21] Conjugation of HYNIC to AnxV is usually done by coupling *N*-succinimidyl-HYNIC to amino groups of the lysine residues. This rather random coupling results in a not clearly defined product as any of the 21 lysine residues can be targeted. As shown by Tait et al. all four domains of AnxV are required for optimal uptake in apoptotic tissues. Therefore caution is necessary in amine-directed labeling strategies that affect multiple residues on the same protein molecule. Previous studies have shown that site-specific labeling methods can considerably improve sensitivity for detecting cell death.[22,23]

Recently our group has developed a novel second generation AnxV derivative with a single cysteine residue at its concave site.[24] This *cys*-AnxV allows site-specific conjugation of different radiometal binding ligands via sulfide formation at the cysteine residue through thiol chemistry. In this way, the introduced chelator is located at a well defined position outside the binding region of the protein, thus not affecting its binding properties. We have derivatized this so-called 'second generation' *cys*-AnxV in different ways. Reaction with maleimide-HYNIC yielded HYNIC-*cys*-AnxV

* Corresponding author. Tel.: +32 16 330446; fax: +32 16 330449.
E-mail address: Alfons.Verbruggen@farm.kuleuven.be (A. Verbruggen).

0968-0896/$ - see front matter © 2009 Elsevier Ltd. All rights reserved.
doi:10.1016/j.bmc.2009.12.021

for labeling with ^{99m}Tc. In this way we could compare the newly designed *cys*-AnxV with the already known AnxV, which also used the HYNIC approach for labeling with ^{99m}Tc.[24] Coupling with maleimide-DTPA offered the possibility to radiolabel the resulting DTPA-*cys*-AnxV with ^{99m}Tc-tricarbonyl ($^{99m}Tc(CO)_3^+$). The $^{99m}Tc(CO)_3^+$ moiety is known for its excellent kinetic stability and can easily be prepared using an IsoLink kit from Covidien.[25,26] In an alternative approach labeling with $^{99m}Tc(CO)_3^+$ was performed on *cys*-AnxV that contained an N-terminal His-tag with six histidine residues. A discussion about potential ligands for labeling with the $^{99m}Tc(CO)_3^+$ moiety and the use of a His-tag can be found elsewhere.[27–29] Biechlin et al. recently described advantages of a labeling of AnxV with $^{99m}Tc(CO)_3^+$.[30] But also their approach (a reaction between free amino residues of lysine and 2-iminothiolane) introduced a chelating group unspecifically as seen for *N*-succinimidyl-HYNIC, contrary to the site-specific conjugation we demonstrate here for the second generation AnxV.

The three novel ^{99m}Tc-labeled AnxV derivatives were all studied in cell binding experiments on Jurkat T-cells, treated with ionomycin. Biodistribution was studied in normal mice as well as in a mouse model for apoptosis (anti-Fas mAb).[31] Based on these experiments the most promising tracer was chosen to demonstrate imaging of apoptosis with μSPECT and to study specific binding.

2. Experimental

2.1. Second generation AnxV derivates

The mutant second generation AnxV was developed by site directed mutagenesis at the University of Maastricht. Glutamine at position 2 was replaced by a cysteine residue and cysteine at position 315 was replaced by serine. The resulting protein with one accessible cysteine residue at position 2 was conjugated with chelating ligands through thiol chemistry. The reaction with 5-maleimido-2-hydraziniumpyridine hydrochloride (maleimide-HYNIC, Abgent, San Diego, CA, USA) formed HYNIC-*cys*-AnxV (**1**). DTPA-*cys*-AnxV (**2**) was formed by reaction of *cys*-AnxV with maleimide-functionalized diethylene triamine pentaacetic acid (maleimide-DTPA, Abgent). His-tagged *cys*-AnxV (**3**) was prepared by cloning cDNA of *cys*-AnxV into pQE30 (Qiagen, KJ Venlo, The Netherlands) in frame and transforming it in E. Coli JM109 with the cloned vector. This resulted in *cys*-AnxV with six histidine amino acids on the N-terminal side of the protein (i.e., at the concave side outside the PS binding region of AnxV). His-tagged *cys*-AnxV was purified from the bacteria using Ni–NTA technology (GE Healthcare-Amersham Pharmacia, Uppsala, Sweden).[32] Then free cysteine was derivatized with maleimide-biotin to offer the possibility for additional histological avidin–biotin staining and to prevent the formation of disulfides.

2.2. Liquid chromatography

Radiolabeled *cys*-AnxV derivatives were analyzed by size exclusion chromatography (BioSep-SEC-S3000 column, 300 mm × 7.8 mm, Phenomenex, Bester, Amstelveen, The Netherlands) using 0.01 M phosphate buffer (pH 7) as mobile phase at a flow rate of 1 ml/min (isocratic). The eluate was monitored for ultraviolet (UV) absorbance (Merck Hitachi LV 4000, Burladingen, Germany) at 254 nm and for radioactivity using a NaI(Tl) scintillation detector.

The main peak (retention time (t_R) = 11.7 min) was isolated and analyzed by sodium dodecylsulfate–polyacrylamide gel electrophoresis (SDS–PAGE). The protein was stained with Coomassie brilliant blue R-250 (CBB) and the labeled compound was detected with a STORM 840 Phosphor Imager (Molecular Dynamics, Sunnyvale, CA, USA), confirming a size of 36 kDa for the labeled compound.

2.3. ^{99m}Tc-HYNIC-*cys*-AnxV (^{99m}Tc-**1**)

Labeling of HYNIC-*cys*-AnxV with technetium-99m was done in a sealed 10-ml nitrogen flushed glass vial. 300 μl of [^{99m}Tc]pertechnetate solution (800–1600 MBq) from an UltraTechnekow ^{99}Mo/^{99m}Tc-generator (Covidien, Petten, The Netherlands) was mixed with 16 μl of 0.02 M citrate buffer, pH 6, 16 μl tricine solution (30 mg/ml in water) and 14 μl $SnCl_2$ solution (1 mg $SnCl_2 \cdot 2H_2O$/ml in 0.05 M HCl). Finally, 50–60 μg of HYNIC-*cys*-AnxV was added and the mixture was incubated at room temperature for 30 min.

Purification and buffer exchange were done with Micron Ultracel YM-10 centrifugal filters (Millipore, Brussels, Belgium) (centrifugation at 12,000 rpm for 15 min followed by two rinse steps with 0.2 ml of 0.9% saline), yielding ^{99m}Tc- HYNIC-*cys*-AnxV (^{99m}Tc-**1**) in 0.9% saline solution.

2.4. $^{99m}Tc(CO)_3$-DTPA-*cys*-AnxV ($^{99m}Tc(CO)_3$-**2**)

The $^{99m}Tc(CO)_3^+$ precursor was prepared by adding 1 ml of [^{99m}Tc]pertechnetate solution (1800–2500 MBq) to an IsoLink kit (Covidien, Petten, The Netherlands) which then was heated at 90 °C for 20 min. $^{99m}Tc(CO)_3^+$ precursor solution (400 μl) was adjusted to pH 7.5 with 1 M HCl and added to 50–60 μg DTPA-*cys*-AnxV. The solution was incubated at 37 °C for 1 h under a stream of nitrogen to reduce the total volume of the reaction mixture. Purification was done as for ^{99m}Tc-HYNIC-*cys*-AnxV to obtain $^{99m}Tc(CO)_3$-**2** in 0.9% saline solution.

2.5. $^{99m}Tc(CO)_3$-HIS-*cys*-AnxV ($^{99m}Tc(CO)_3$-**3**)

The $^{99m}Tc(CO)_3^+$ precursor solution was prepared as described above (pH 7.5) and 400 μl of it was added to 50–60 μg his-*cys*-AnxV. The solution was incubated at 37 °C for 1 h under a stream of nitrogen to reduce the total volume of the reaction mixture. Purification was done as for ^{99m}Tc-HYNIC-*cys*-AnxV to obtain $^{99m}Tc(CO)_3$-**3** in 0.9% saline solution.

2.6. Stability tests

Samples of ^{99m}Tc-**1**, $^{99m}Tc(CO)_3$-**2** and $^{99m}Tc(CO)_3$-**3** were tested for their plasma stability. The purified tracers (in 100 μl 0.9% saline solution) were mixed with 1 ml of human plasma and the mixtures were kept at 37 °C. One to four hours later the composition was checked with size exclusion chromatography (SEC). For the $^{99m}Tc(CO)_3$-complexes ($^{99m}Tc(CO)_3$-**2** and **3**) a competition reaction with histidine was performed. An excessive amount of histidine (10 mM) was incubated with $^{99m}Tc(CO)_3$-**2** and with $^{99m}Tc(CO)_3$-**3** for 1 h after which the mixtures were analyzed using SEC-HPLC.

2.7. In vitro binding assay

Binding capacity of the three ^{99m}Tc-labeled *cys*-AnxV products to PS was checked in vitro with ionomycin treated Jurkat cells.[33,34]

Jurkat T-lymphocyte cells were cultured in RPMI 1640 medium with glutamax I, 10% fetal bovine serum (FBS) and 1% penicillin/streptomycin (P/S). Culture plates were incubated at 37 °C in humidified air with 5% carbon dioxide, and kept in logarithmic phase by routine passage every 2–3 days. Cells were counted with a bürker abacus. Cells were centrifuged at 300*g* for 3 min before being resuspended in fresh medium (10 mM Hepes, pH 7.4; 150 mM NaCl; 5 mM KCl; 1 mM $MgCl_2$; 1 mg/ml BSA) at 10^6 cells/ml. Cells were incubated for 10 min with ionomycin

(2 μM), a calcium ionophor. This results in development of an intracellular calcium concentration up to 1 μM, nearly 10 times higher than that seen during apoptosis, and a massive PS externalization.[34] Threefold ($n = 3$) ionomycin treated cells (5×10^5) and threefold ($n = 3$) non-treated cells were incubated for 15 min with radiolabeled AnxV (50 ng) in an Eppendorf tube. Afterward the Eppendorf tubes were centrifuged for 2 min at 1000*g*. The supernatant was removed from the pellet and the activities were measured using a gamma counter. The percentage of cell-bound activity was expressed as the percentage of radioactivity in the pellet to the total radioactivity. Ratios of radioactivity in treated cells compared to radioactivity in non-treated cells were calculated.

2.8. Animals

Studies in animals were conducted under a protocol approved by the ethics committee for animal experiments of the University of Leuven. For the biodistribution experiments and for the FAS-mediated hepatic apoptosis model normal wild type NMRI mice were used.

2.9. Biodistribution studies

Biodistribution studies were performed in normal NMRI mice after tail vein injection of 750–1800 kBq purified ^{99m}Tc-labeled *cys*-AnxV under isoflurane anesthesia. Animals were sacrificed at 1 h or 4 h pi (3–4 per time point). Organs were weighed and their radioactivity measured in an automated NaI(Tl) gamma counter (Wallac Wizard, Turku, Finland). Uptake is expressed as percentage of injected dose (% ID)/organ and % ID/g of organ.

2.10. In vivo model of Fas-mediated hepatic apoptosis

Fas is a death receptor belonging to the tumor necrosis factor (TNF) receptor gene family. The 'death inducing' Fas ligand binds to three Fas receptors on the surface of a target cell resulting in a clustering of the receptors' death domains (DDs). Then the cytosolic adapter protein FADD is recruited which activates the initiator caspase-8, inducing apoptosis through the effector caspases.[35]

Intravenous injection of an anti-Fas monoclonal antibody (mAb) in mice induces rapid and massive apoptosis in the liver.[31] NMRI mice were injected intravenously (iv) under isoflurane anesthesia with purified hamster anti-Fas mAb (7–10 μg of anti-Fas mAb per mouse, Jo2, BD Pharmingen, Erembodegem, Belgium). 90 min later mice ($n = 3$) were iv injected with 750 kBq of ^{99m}Tc-labeled *cys*-AnxV (^{99m}Tc-**1**, ^{99m}Tc(CO)$_3$-**2** or ^{99m}Tc(CO)$_3$-**3**). Parallel non-treated mice (control, $n = 3$) were injected with the same activity of radioactive tracer. All animals were sacrificed and dissected 1 h pi and the activity of the weighed organs was measured in an automated NaI(Tl) gamma counter to calculate the percentage of ID. Data were expressed as % ID/organ or % ID/g of organ.

Part of the liver was frozen for autoradiography, the other part fixed in 6% formaldehyde for paraffin embedding and histological staining. Autoradiographs were recorded from frozen coronal sections of liver tissue (30 or 50 μm thick) using a phosphor storage screen (Canberra-Packard, Meriden, CT, USA), exposed overnight in a cassette (Kodak, Zaventem, Belgium). The exposed screen was then read using a Cyclone plus storage phosphor system (Storage Phosphor System, Perkin-Elmer, Downers Grove, IL, USA).

Five-micrometer sections were cut from paraffin embedded livers for histological staining. Standard hematoxylin and eosin (H&E) staining was performed. In H&E stained slices apoptotic cells are defined as small cells with dense chromatin (condensation) or in a later stage through the formation of apoptotic bodies. Immunostaining was performed with caspase-3 antibody (Cell Signaling, Bioké, Leiden, The Netherlands). Also terminal deoxynucleotidyl transferase biotin-dUTP nick end labeling (TUNEL) was performed. All histological stainings were scored semi-quantitatively and the fraction of stained cells was expressed as a percentage of the total number of liver cells per defined field of view.

Additionally immunostaining of the excised liver tissue using a polyclonal antibody against AnxV (Hyphen Biomed, Villejuif, France) was performed to show specific binding of injected ^{99m}Tc-labeled AnxV to the plasma membrane of cells with apoptotic morphology.

2.11. In vivo imaging of Fas-mediated hepatic apoptosis

Images were acquired using a standard SPECT camera (E-cam, Siemens Medical Systems, Hoffman Estates, IL, USA). The camera was equipped with two pinhole collimators having multi-pinhole removable plates optimized for focused mouse imaging with high sensitivity.[36] The plates have seven holes with a diameter of 1.5 mm. The intrinsic resolution of the detectors is 4 mm and the spatial resolution is 1.2 mm thanks to the magnification of the pinholes.[37] Acquisition was completed in 35 min with 64 projections taken over 360° in a step-and-shoot mode (30 s per projection angle). During reconstruction images were corrected for scatter and decay. Further post-correction for the injected dose and the weight of the mouse delivered standardized uptake values (SUVs). To enable image comparison, the images were clipped to the same maximum.

Two NMRI mice were imaged 1 h after injection of 15 MBq of ^{99m}Tc(CO)$_3$-**3** (=baseline μSPECT). After two days the same mice were treated with anti-Fas mAb (7 μg) and 90 min later 15 MBq of ^{99m}Tc(CO)$_3$-**3** was injected. μSPECT was performed 1 h later (=post-treatment μSPECT). Blocking of PS binding to apoptotic hepatocytes was investigated by pre-injection of cold AnxV. Two NMRI mice were treated with anti-Fas and 60 min later 2 mg of cold unmodified AnxV was injected to block specific binding and to confirm thereby the specificity of ^{99m}Tc-labeled *cys*-AnxV uptake in the liver. ^{99m}Tc(CO)$_3$-**3** was injected 30 min later and after 1 h μSPECT images were acquired (=blocking μSPECT). The mice were then sacrificed under anesthesia, radioactivity in the dissected liver was measured and autoradiography performed.

2.12. Statistical analysis

All values are shown as mean ± SD. Statistical significance between two groups was tested by unpaired Student's *t*-test using the software STATISTICA 6.0 (StatSoft, Groningen, The Netherlands). A 2-tailed value of $p < 0.05$ was considered to be statistically significant.

3. Results and discussion

3.1. Radiolabeling and stability

Radiolabeling yield for ^{99m}Tc-**1** was $\geqslant$85%. Radiochemical impurities eluting from the column later than radiolabeled AnxV such as ^{99m}Tc-tricine-citrate ($t_R = 13.5$ min) and [^{99m}Tc]pertechnetate ($t_R = 21$ min) could not be avoided under optimized conditions. However, an efficient purification method with YM-10 centrifugal filters was introduced to isolate the labeled product (>98% purity). ^{99m}Tc(CO)$_3$-**2** and ^{99m}Tc(CO)$_3$-**3** both had radiochemical yields >90% (Fig. 1), opening up favorable perspectives for the development of a (clinical) kit. Unconjugated ^{99m}Tc(CO)$_3$ precursor ($t_R = 13.5$ min) was removed by centrifugation resulting in products with a purity >98%.

^{99m}Tc-**1** remained unchanged as a single compound after 4 h in plasma. After 1.5 h in plasma 70% of $^{-99m}$Tc(CO)$_3$-**2** was still present. A small peak was formed which eluted before that of ^{99m}Tc-

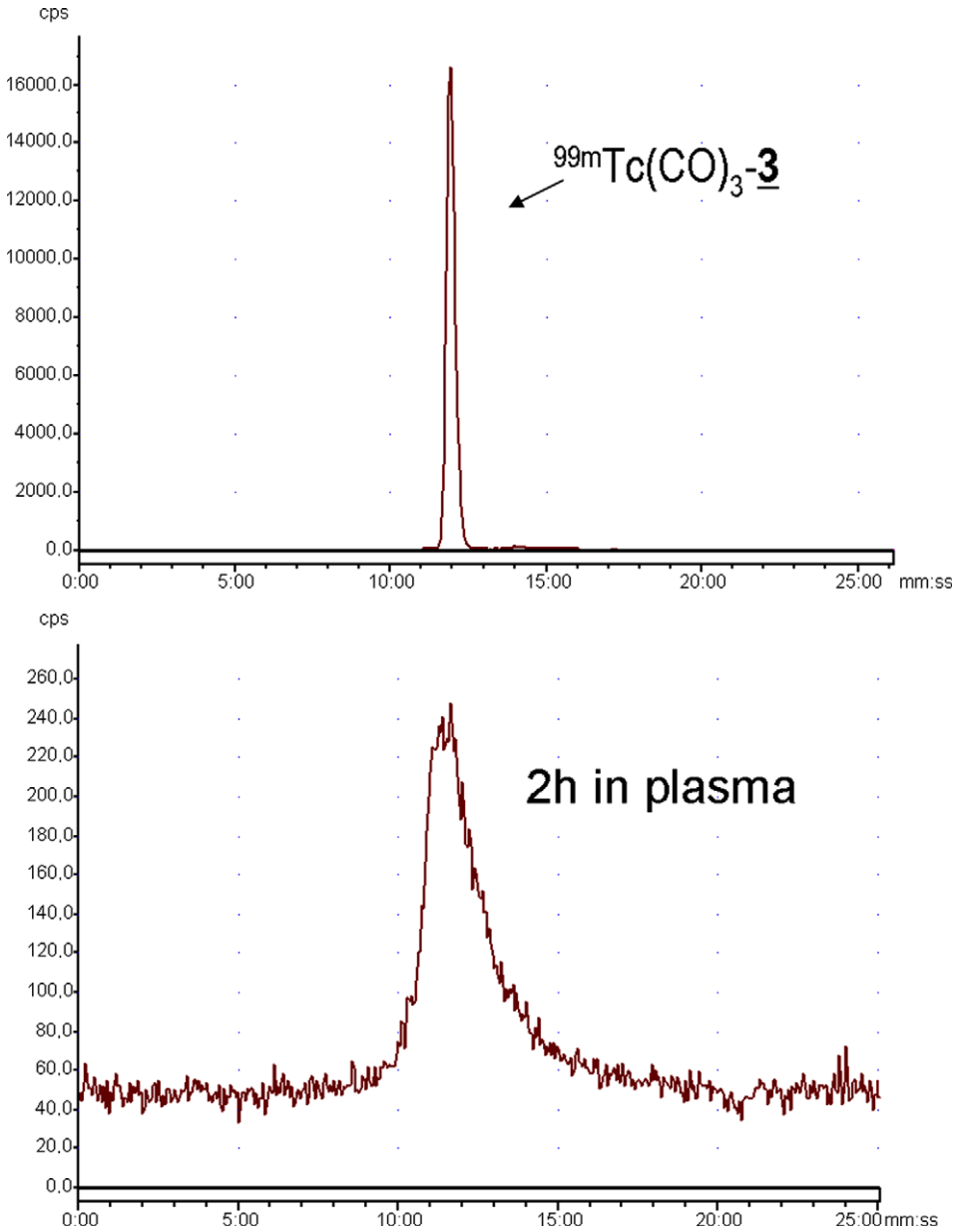

Figure 1. SEC-HPLC chromatogram of the reaction mixture after labeling of his-*cys*-AnxV with $^{99m}Tc(CO)_3$ (A). >98% of the activity elutes in the form of $^{99m}Tc(CO)_3$-**3** (t_R = 11.7). The plasma stability of $^{99m}Tc(CO)_3$-**3** after 2 h is shown in the lower chromatogram (B).

cys-AnxV, representing compounds of higher molecular mass. Later time points in plasma were not checked for these tracers. The competition reaction with an excess of histidine showed a shift of at least 30% of the ^{99m}Tc-label from the DTPA-*cys*-AnxV to histidine.

$^{99m}Tc(CO)_3$-**3** remained unchanged in plasma, as shown by the single peak on SEC-HPLC after 2 h in plasma (Fig. 1). $^{99m}Tc(CO)_3$-**3** remained also unchanged in the presence of an excess of histidine, demonstrating the excellent stability of the compound. These results suggest that DTPA is not an ideal chelating ligand for the $^{99m}Tc(CO)_3^+$ core in this setup, while $^{99m}Tc(CO)_3$-**3** was found to be a remarkably stable complex.

3.2. In vitro binding assay

In vitro binding characteristics of ^{99m}Tc-**1**, $^{99m}Tc(CO)_3$-**2** and $^{99m}Tc(CO)_3$-**3** were studied to prove that the PS binding capacity is maintained after derivatization and radiolabeling of the respective AnxV derivatives under the described conditions. All three tracers were found to have a significantly higher uptake in ionomycin treated cells compared to non-treated cells (Fig. 2).

^{99m}Tc-**1** had twice the percentage of radioactivity (ratio of 2 ± 0.1) in the pellet for the treated cells (44.3 ± 6.4%) compared to non-treated cells (22.1 ± 2.5%) (p = 0.005) (Fig. 2).

$^{99m}Tc(CO)_3$-**2** had twice the percentage of radioactivity (ratio of 2.2 ± 0.2) in the pellet for the treated cells (31.2 ± 7.6%) compared to non-treated cells (14.3 ± 3.6%) (p = 0.01) (Fig. 2).

$^{99m}Tc(CO)_3$-**3** had more than three times the percentage of radioactivity (ratio of 4.2 ± 0.6) in the pellet for the treated cells (50 ± 5.7%) compared to the non-treated cells (12 ± 0.8%) (p = 0.003) (Fig. 2). These results demonstrate that the derivatization and labeling of AnxV did not disturb PS binding for the three radiotracers. Although $^{99m}Tc(CO)_3$-**3** looks more promising the experiment is limited to draw a final conclusion. It is remarkable that the controls show high and different radioactivity in the pellet. The high radioactivity is most likely due to non-specific sticking of AnxV to the walls of the Eppendorf tube. We used a simple method

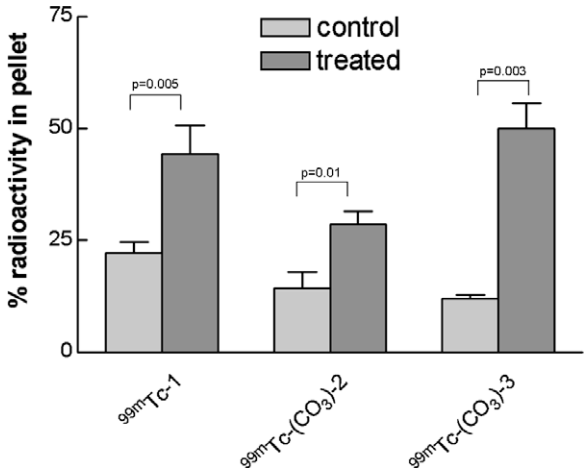

Figure 2. Histogram representation of in vitro binding experiment. The percentage of radioactivity in the pellet is shown for ^{99m}Tc-**1**, ^{99m}Tc(CO)$_3$-**2** and ^{99m}Tc(CO)$_3$-**3** in non-treated cells (control) and after treatment of the Jurkat cells with ionomycin (treated). For all three tracers the percentage of radioactivity in the pellet is significantly increased for the treated cells in comparison to control cells.

to qualitatively show that the compound still worked. More extensive experiment would be necessary to measure the PS affinity which was beyond the scope of the current sudy.[38]

3.3. Biodistribution in healthy mice

Biodistribution of ^{99m}Tc-**1**, ^{99m}Tc(CO)$_3$-**2** and ^{99m}Tc(CO)$_3$-**3** was determined in normal NMRI mice at 1 and 4 h pi. All ^{99m}Tc-tracers were cleared mainly via the urinary tract (Table 1). A faster urinary excretion was shown for ^{99m}Tc(CO)$_3$-**3** compared to ^{99m}Tc(CO)$_3$-**2** and ^{99m}Tc-**1**. The cortical kidney uptake shown for ^{99m}Tc-**1** on autoradiography (results not shown) and for ^{99m}Tc(CO)$_3$-**3** on μSPECT (Fig. 5) results from high PS expression in the cortex of the kidneys.[39] This was already proposed by Blankenberg who also suggested the possibility of non-specific uptake of low-molecular weight proteins by the proximal renal tubule cells as noted in studies of radiolabeled peptides and antibody fragments.[14,40,41] Hepatobilliary excretion was found for all three ^{99m}Tc-tracers. There was no significant change in liver uptake of the ^{99m}Tc-tracers from 1 to 4 h after injection. ^{99m}Tc-**1** uptake in the liver after 4 h was significantly lower than that of ^{99m}Tc(CO)$_3$-**2** and ^{99m}Tc(CO)$_3$-**3** (Table 1). A clear stomach uptake was seen for ^{99m}Tc-**1** which suggests a partial oxidation of ^{99m}Tc and formation of $^{99m}TcO_4^-$. This was not observed for both ^{99m}Tc(CO)$_3$ tracers. Blood clearance was fastest for ^{99m}Tc-**1**. ^{99m}Tc(CO)$_3$-**2** and ^{99m}Tc(CO)$_3$-**3** stayed longer in the blood although their residual retention in blood decreased gradually from 1 to 4 h. An advantage of fast clearance is the resulting low background activity, but a longer circulating tracer might have more chance of binding the target as in case of ^{99m}Tc(CO)$_3$-**2** and ^{99m}Tc(CO)$_3$-**3.**

A recently published study by Fonge et al. demonstrated a similar biodistribution for first generation ^{99m}Tc-HYNIC-AnxV and the second generation ^{99m}Tc-HYNIC-*cys*-AnxV.[24] However, the biodistribution results of the present study for ^{99m}Tc-**1** at 1 h after injection differ from the data given in Fonge's study. The labeling method was the same in both studies, but in the present study a centrifugal purification method was introduced as compared to SEC purification in the study of Fonge et al.[24] A decreased uptake in liver, lungs, spleen and heart was seen for ^{99m}Tc-**1** and also a lower retention in blood after 1 h (0.96 ± 0.49% ID/g compared to 2.9 ± 0.2% ID/g). SEC-purification necessitates manipulation of the protein during a longer time and reduction of the volume after collection of the desired HPLC peak by gentle heating under a stream of nitrogen. These conditions might result in colloid formation and therefore more lung uptake. Also the different ionic strength of the solvents used for SEC purification and centrifugal purification (0.01 M phosphate buffer vs 0.9% saline) might contribute to the differing results, especially as the salt concentration increases when the volume is reduced. Purification using centrifugal filters thus may have the advantage of decreasing background activity.

3.4. Fas-mediated hepatic apoptosis

Previous studies demonstrated the lethal effect of anti-Fas mAb on hepatocytes.[31] However, ex vivo quantification of apoptosis by H&E, TUNEL and caspase-3 has not yet been reported before and are shown in Table 2. Both TUNEL and H&E detect DNA fragmentation and apoptotic bodies occurring late in the process of apoptosis and give similar levels of apoptosis after treatment (±20%) (Fig. 3C, D, G, and H). Caspase-3 is activated early in the process and therefore immunostaining with caspase-3 antibody showed a greater number of apoptotic cells after treatment (60%) (Fig. 3K and L). These results demonstrate that treatment with anti-Fas mAb leads to a fast hepatic apoptosis with more than half of the hepatocytes becoming apoptotic within 150 min. Immunostaining of AnxV (brown color) revealed little AnxV presence in normal livers

Table 2
Liver uptake of ^{99m}Tc-(**1**), ^{99m}Tc(CO)$_3$-(**2**) and ^{99m}Tc(CO)$_3$-(**3**) in normal and anti-Fas treated NMRI mice (n = 3) at 1 h pi expressed as % ID/g. Rate of apoptosis assessed using H&E staining, caspase-3 staining and TUNEL in normal and anti-Fas treated livers

	Normal	Anti-Fas
% ID/g of ^{99m}Tc-(**1**)	5.2 ± 1.3	15.3 ± 4.4
% ID/g of ^{99m}Tc(CO)$_3$-(**2**)	4.8 ± 0.4	7 ± 0.7
% ID/g of ^{99m}Tc(CO)$_3$-(**3**)	6.8 ± 0.8	28.9 ± 3.4
% Apoptotic cells with H&E	0.3 ± 0.1	18.3 ± 4.0
% TUNEL positive	0.8 ± 0.3	20.9 ± 7.4
% Caspase-3 positive	0.3 ± 0.1	63.8 ± 4.2

Table 1
Biodistribution of ^{99m}Tc-(**1**), ^{99m}Tc(CO)$_3$-(**2**) and ^{99m}Tc(CO)$_3$-(**3**) in normal NMRI mice 1 and 4 h post-injection (pi) expressed as % ID/g (n = 3 or 4)

% ID/g	^{99m}Tc-(1)		^{99m}Tc(CO)$_3$-(2)		^{99m}Tc(CO)$_3$-(3)	
	1 h pi	4 h pi	1 h pi	4 h pi	1 h pi	4 h pi
Kidneys	59.2 ± 12.1	47.2 ± 6.3	70.2 ± 7.6	44.3 ± 0.5	42.4 ± 5.1	37 ± 9.6
Liver	5.2 ± 1.3	3.7 ± 0.6	7.5 ± 1.9	6.4 ± 0.3	6.7 ± 0.9	8.4 ± 3
Spleen	3.4 ± 1.1	3.6 ± 0.9	5.6 ± 3.4	2.6 ± 1.2	5 ± 1.4	3.1 ± 0.9
Lungs	3.5 ± 0.6	1.4 ± 0.2	4.2 ± 0.2	2.9 ± 0.1	11.5 ± 3.7	9.5 ± 5.7
Heart	1.3 ± 0.3	0.5 ± 0.1	1.7 ± 0.03	1.2 ± 0.1	1.6 ± 0.4	1.4 ± 0.6
Intestines	1.3 ± 0.3	1.7 ± 0.1	1.2 ± 0.3	1.3 ± 0.1	0.8 ± 0.1	2 ± 0.2
Stomach	8.3 ± 2	4.6 ± 1.6	0.6 ± 0.5	0.9 ± 0.3	1 ± 0.2	1.1 ± 0.4
Blood	1 ± 0.5	0.5 ± 0.1	3.8 ± 0.7	2.1 ± 0.1	2.9 ± 0.4	1.6 ± 0.5

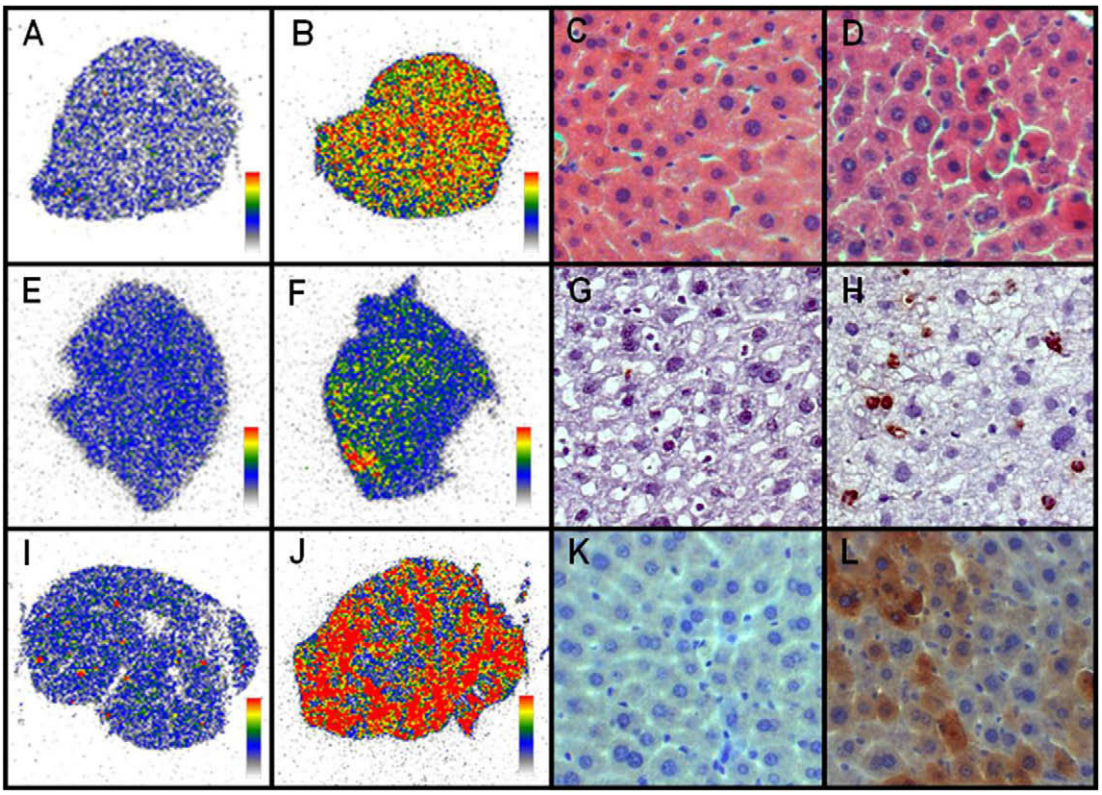

Figure 3. Autoradiography images of liver of normal and anti-Fas mAb treated mice after injection of ^{99m}Tc-**1** (A and B), ^{99m}Tc(CO)$_3$-**2** (E and F), ^{99m}Tc(CO)$_3$-**3** (I and J). Stainings of normal (C, G, and K) and anti-Fas treated (D, H, and L) livers with H&E, TUNEL and caspase-3, respectively.

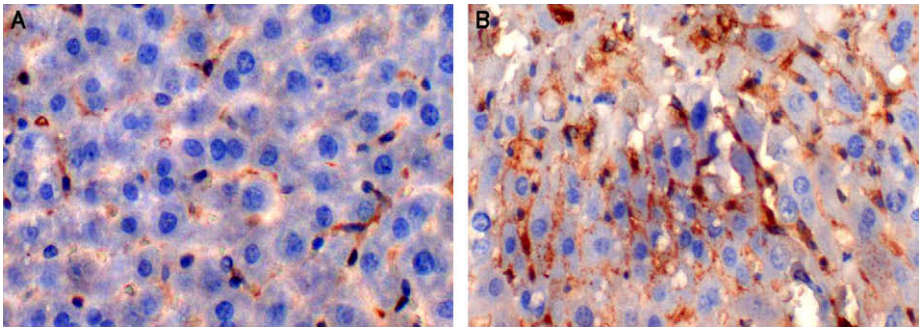

Figure 4. Immunostaining of liver of normal mouse (A) and anti-Fas treated mouse (B) using a polyclonal antibody against AnxV-V (brown color). This visualizes the binding of AnxV to the membrane of apoptotic cells.

(Fig. 4A) while anti-Fas treated livers showed AnxV binding to the cell membranes of apoptotic cells (Fig. 4B).

Uptake of ^{99m}Tc-**1** and ^{99m}Tc(CO)$_3$-**2** was significantly ($p = 0.003$ and $p = 0.007$, respectively) higher in liver of anti-Fas mAb treated animals compared to controls (Table 2). Autoradiography showed a 3.6 and 1.5 times higher liver uptake of ^{99m}Tc-**1** and ^{99m}Tc(CO)$_3$-**2**, respectively, after treatment (Fig. 3A, B, E, and F).

^{99m}Tc(CO)$_3$-**3** showed the highest liver uptake of the three ^{99m}Tc-labeled AnxV derivatives in anti-Fas mAb treated animals. It was significantly increased ($p < 0.0001$) from 6.8 ± 0.8% ID/g to 28.9 ± 3.4% ID/g (Table 2). Autoradiography also revealed a 4.8 times higher liver uptake of ^{99m}Tc(CO)$_3$-**3** after treatment as compared to control mice (Fig. 3I and J). These results show the ability of ^{99m}Tc-labeled second generation AnxV mutants to bind to apoptotic cells in vivo, with the best result for ^{99m}Tc(CO)$_3$-**3** (Fig. 3). The ^{99m}Tc(CO)$_3$-**3** revealed a 61% higher affinity for apoptosis in comparison to the first generation ^{99m}Tc-HYNIC-AnxV which was evaluated in the same anti-Fas model and showed an only 2.6 times higher liver uptake after treatment.[24] As the ^{99m}Tc(CO)$_3$-**3** compound has a higher bloodpool value (discussed under Section 3.3) it should be noted that the target-to-blood ratios are in the same order of magnitude compared to ^{99m}Tc-**1**. Although it was not reflected in our images this could be approached by delaying the time between ^{99m}Tc(CO)$_3$-**3** injection and acquisition. In the current setting we could not investigate this with the anti-Fas model since animals die approximately 4 h after treatment.

μSPECT images acquired after administration of ^{99m}Tc(CO)$_3$-**3** to normal mice showed very high uptake in the kidneys (especially coronal uptake) and some liver uptake (Fig. 5A and B). Mice treated with anti-Fas mAb displayed mainly liver uptake and much less activity in the kidneys 1 h after ^{99m}Tc(CO)$_3$-**3** injection (Fig. 5C and D). The pre-injection of cold unmodified AnxV caused a decreased uptake in the apoptotic liver (Fig. 5E and F) as compared to the liver of anti-Fas treated mice not pre-treated with cold AnxV (Fig. 5C and D). This proves that PS binding sites were saturated and ^{99m}Tc(CO)$_3$-**3** uptake in the apoptotic liver was exclusively due to the protein characteristics.

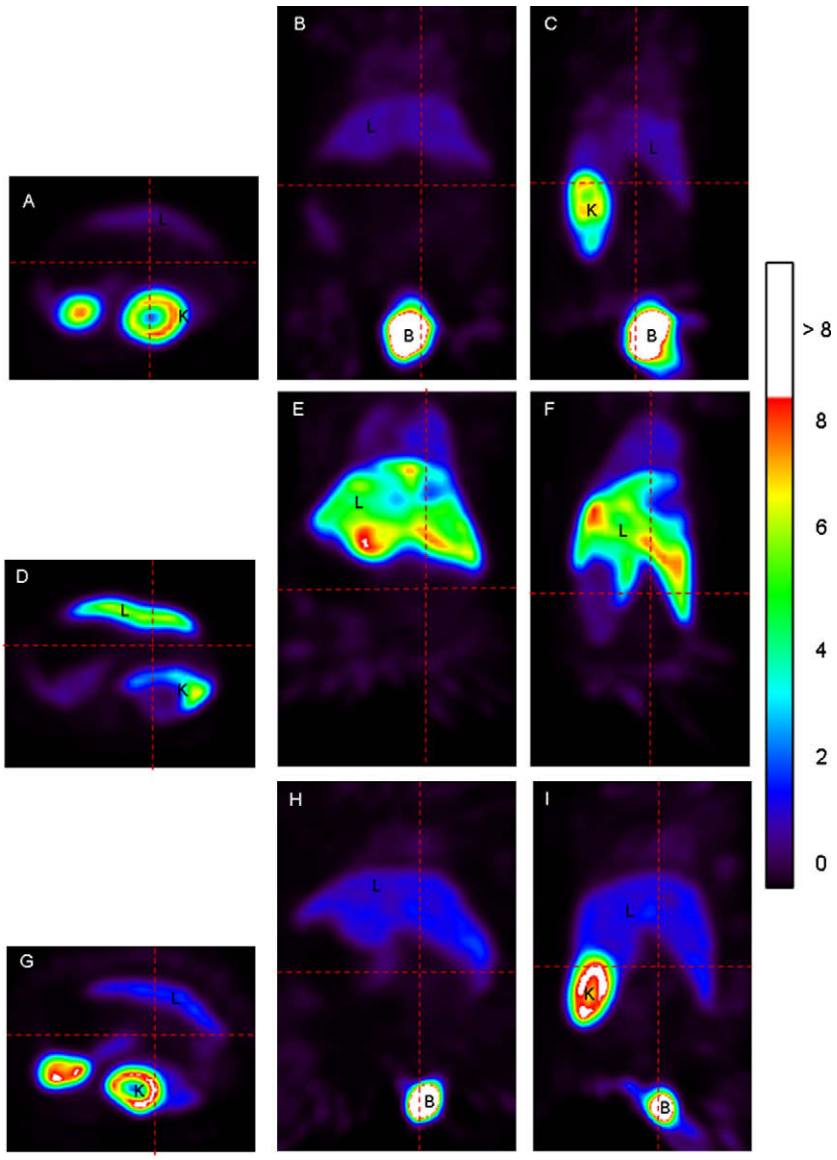

Figure 5. μSPECT imaging 1 h after $^{99m}Tc(CO)_3$-**3** injection in mice. Image values are expressed as SUV and the same scaling is used for the different acquisitions. Imaging was performed before treatment (A–C), after treatment with anti-Fas (D–F) and after treatment with anti-Fas and pre-injection of cold AnxV (G–I). Transversal (A, D, and G), coronal (B, E, and H) and sagittal (C, F, and I) views are shown. Liver, kidneys and bladder are indicated by L, K, B.

4. Conclusion

Second generation *cys*-AnxV derivatives were successfully labeled to form three apoptosis imaging agents (^{99m}Tc-**1**, $^{99m}Tc(CO)_3$-**2** and $^{99m}Tc(CO)_3$-**3**). $^{99m}Tc(CO)_3$-**3** showed the best results with respect to radiolabeling yields (kit formulation possible), stability, distribution in the body (fast urinary elimination, low stomach uptake, etc.) and in vivo affinity for hepatic apoptosis. The low target-to-background activity ratio experienced in clinical imaging applications with first generation ^{99m}Tc-HYNIC-AnxV[19–21] might be improved with this second generation $^{99m}Tc(CO)_3$-**3**. This can open new opportunities for an early tumor response assessment in cancer patients.

Acknowledgments

We thank Peter Vermaelen, Ellen Devos and Hubert Vanbilloen for their practical help in this study. We also acknowledge Covidien for kindly providing us with IsoLink kits. This research was supported by the Euregional PACT Project 4-BMG-II-2=70 and EC-FP6-Project DiMI. A further grant was received from the Center of Excellence MoSAIC, KU Leuven.

References

1. Kerr, J. F.; Wyllie, A. H.; Currie, A. R. *Br. J. Cancer* **1972**, *26*(4), 239.
2. Thompson, C. B. *Science* **1995**, *267*(5203), 1456.
3. Blankenberg, F. G.; Strauss, H. W. *Pediatr. Radiol.* **1999**, *29*(5), 299.
4. Freude, B.; Masters, T. N.; Kostin, S.; Robicsek, F.; Schaper, J. *Basic Res. Cardiol.* **1998**, *93*(2), 85.
5. D'Arceuil, H.; Rhine, W.; de, C. A.; Yenari, M.; Tait, J. F.; Strauss, W. H.; Engelhorn, T.; Kastrup, A.; Moseley, M.; Blankenberg, F. *Stroke* **2000**, *31*(11), 2692.
6. Blankenberg, F. G.; Strauss, H. W. A. *Apoptosis* **2001**, *6*(1–2), 117.
7. Hersey, P.; Zhang, X. D. *J. Cell. Physiol.* **2003**, *196*(1), 9.
8. Neves, A. A.; Brindle, K. M. *Biochim. Biophys. Acta* **2006**, *1766*(2), 242.
9. Fadok, V. A.; Voelker, D. R.; Campbell, P. A.; Cohen, J. J.; Bratton, D. L.; Henson, P. M. *J. Immunol.* **1992**, *148*(7), 2207.
10. Boersma, H. H.; Kietselaer, B. L.; Stolk, L. M.; Bennaghmouch, A.; Hofstra, L.; Narula, J.; Heidendal, G. A.; Reutelingsperger, C. P. *J. Nucl. Med.* **2005**, *46*(12), 2035.
11. Gerke, V.; Moss, S. E. *Physiol. Rev.* **2002**, *82*(2), 331.
12. Martin, S. J.; Reutelingsperger, C. P.; McGahon, A. J.; Rader, J. A.; van Schie, R. C.; LaFace, D. M.; Green, D. R. *J. Exp. Med.* **1995**, *182*(5), 1545.

13. Blankenberg, F. G.; Katsikis, P. D.; Tait, J. F.; Davis, R. E.; Naumovski, L.; Ohtsuki, K.; Kopiwoda, S.; Abrams, M. J.; Darkes, M.; Robbins, R. C.; Maecker, H. T.; Strauss, H. W. *Proc. Natl. Acad. Sci. U.S.A.* **1998**, *95*(11), 6349.
14. Blankenberg, F. G.; Katsikis, P. D.; Tait, J. F.; Davis, R. E.; Naumovski, L.; Ohtsuki, K.; Kopiwoda, S.; Abrams, M. J.; Strauss, H. W. *J. Nucl. Med.* **1999**, *40*(1), 184.
15. Zhang, G.; Gurtu, V.; Kain, S. R.; Yan, G. *Biotechniques* **1997**, *23*(3), 525.
16. Hofstra, L.; Liem, I. H.; Dumont, E. A.; Boersma, H. H.; van Heerde, W. L.; Doevendans, P. A.; De, M. E.; Wellens, H. J.; Kemerink, G. J.; Reutelingsperger, C. P.; Heidendal, G. A. *Lancet* **2000**, *356*(9225), 209.
17. Belhocine, T.; Steinmetz, N.; Hustinx, R.; Bartsch, P.; Jerusalem, G.; Seidel, L.; Rigo, P.; Green, A. *Clin. Cancer Res.* **2002**, *8*(9), 2766.
18. Belhocine, T.; Steinmetz, N.; Li, C.; Green, A.; Blankenberg, F. G. *Technol. Cancer Res. Treat.* **2004**, *3*(1), 23.
19. Rottey, S.; Loose, D.; Vakaet, L.; Lahorte, C.; Vermeersch, H.; Van, B. S.; Van de, W. C. *Q. J. Nucl. Med. Mol. Imaging* **2007**, *51*(2), 182.
20. Rottey, S.; Slegers, G.; Van, B. S.; Goethals, I.; Van de, W. C. *J. Nucl. Med.* **2006**, *47*(11), 1813.
21. Kartachova, M.; van, Z. N.; Burgers, S.; van, T. H.; Verheij, M.; Valdes Olmos, R. A. *J. Clin. Oncol.* **2007**, *25*(18), 2534.
22. Tait, J. F.; Smith, C.; Levashova, Z.; Patel, B.; Blankenberg, F. G.; Vanderheyden, J. L. *J. Nucl. Med.* **2006**, *47*(9), 1546.
23. Tait, J. F.; Smith, C.; Blankenberg, F. G. *J. Nucl. Med.* **2005**, *46*(5), 807.
24. Fonge, H.; De Saint Hubert, M.; Vunckx, K.; Rattat, D.; Nuyts, J.; Bormans, G.; Ni, Y.; Reutelingsperger, C.; Verbruggen, A. *Bioorg. Med. Chem. Lett.* **2008**, *18*(13), 3794.
25. Alberto, R.; Schibli, R.; Waibel, R.; Abram, U.; Schubiger, A. P. *Coord. Chem. Rev.* **1999**, *190–192*, 901.
26. Schibli, R.; Schwarzbach, R.; Alberto, R.; Ortner, K.; Schmalle, H.; Dumas, C.; Egli, A.; Schubiger, P. A. *Bioconjugate Chem.* **2002**, *13*(4), 750.
27. Rattat, D.; Terwinghe, C.; Verbruggen, A. *Tetrahedron* **2005**, *61*, 9563.
28. Waibel, R.; Alberto, R.; Willuda, J.; Finnern, R.; Schibli, R.; Stichelberger, A.; Egli, A.; Abram, U.; Mach, J. P.; Pluckthun, A.; Schubiger, P. A. *Nat. Biotechnol.* **1999**, *17*(9), 897.
29. Rattat, D.; Eraets, K.; Cleynhens, B.; Knight, H.; Fonge, H.; Verbruggen, A. *Tetrahedron Lett.* **2004**, *45*(12), 2531.
30. Biechlin, M. L.; Bonmartin, A.; Gilly, F. N.; Fraysse, M.; du Moulinet, d. A. *Nucl. Med. Biol.* **2008**, *35*(6), 679.
31. Ogasawara, J.; Watanabe-Fukunaga, R.; Adachi, M.; Matsuzawa, A.; Kasugai, T.; Kitamura, Y.; Itoh, N.; Suda, T.; Nagata, S. *Nature* **1993**, *364*(6440), 806.
32. Loo, T. W.; Clarke, D. M. *J. Biol. Chem.* **1995**, *270*(37), 21449.
33. Hampton, M. B.; Vanags, D. M.; Porn-Ares, M. I.; Orrenius, S. *FEBS Lett.* **1996**, *399*(3), 277.
34. Park, H. J.; Makepeace, C. M.; Lyons, J. C.; Song, C. W. *Eur. J. Cancer A* **1996**, *32*(3), 540.
35. Ashkenazi, A.; Dixit, V. M. *Science* **1998**, *281*(5381), 1305.
36. Vunckx, K.; Nuyts, J.; Vanbilloen, H.; De Saint-Hubert, M.; Vanderghinste, D.; Rattat, D.; Mottaghy, F.; Defrise, M. Optimized multipinhole design for mouse imaging. In *Conference Record of the IEEE Nucl. Sci. Symp. and Med. Imag. Conf. Dresden, Germany*, 2008.
37. Vunckx, K.; Beque, D.; Defrise, M.; Nuyts, J. *IEEE Trans. Med. Imaging* **2008**, *27*(1), 36.
38. Li, X.; Link, J. M.; Stekhova, S.; Yagle, K. J.; Smith, C.; Krohn, K. A.; Tait, J. F. *Bioconjugate Chem.* **2008**, *19*(8), 1684.
39. Sterin-Speziale, N.; Kahane, V. L.; Setton, C. P.; Fernandez, M. C.; Speziale, E. H. *Lipids* **1992**, *27*(1), 10.
40. Kobayashi, H.; Yoo, T. M.; Kim, I. S.; Kim, M. K.; Le, N.; Webber, K. O.; Pastan, I.; Paik, C. H.; Eckelman, W. C.; Carrasquillo, J. A. *Cancer Res.* **1996**, *56*(16), 3788.
41. Lang, L.; Jagoda, E.; Wu, C.; Brechbiel, M. W.; Gansow, O. A.; Pastan, I.; Paik, C. H.; Carrasquillo, J. A.; Eckelman, W. C. *Q. J. Nucl. Med.* **1997**, *41*(2), 53.